

Research Articles: Systems/Circuits

Mapping the integration of sensory information across fingers in human sensorimotor cortex

<https://doi.org/10.1523/JNEUROSCI.2152-21.2022>

Cite as: J. Neurosci 2022; 10.1523/JNEUROSCI.2152-21.2022

Received: 27 October 2021

Revised: 11 April 2022

Accepted: 11 May 2022

This Early Release article has been peer-reviewed and accepted, but has not been through the composition and copyediting processes. The final version may differ slightly in style or formatting and will contain links to any extended data.

Alerts: Sign up at www.jneurosci.org/alerts to receive customized email alerts when the fully formatted version of this article is published.

Mapping the integration of sensory information across fingers in human sensorimotor cortex

Spencer A. Arbuckle¹, J. Andrew Pruszynski^{1,2,3}, Jörn Diedrichsen^{1,4}

1. The Brain and Mind Institute, Western University, London, ON, Canada
2. Departments of Physiology and Pharmacology, & Psychology, Western University, London, ON, Canada
3. Robarts Research Institute, Western University, London, ON, Canada
4. Departments of Statistical and Actuarial Sciences, & Computer Science, Western University, London, ON, Canada

Correspondence:

Jörn Diedrichsen (jdiedric@uwo.ca) & Spencer Arbuckle (saruck3@uwo.ca)

Abbreviated title: Integration of sensory information across fingers

Length: 33 pages (clean version), Abstract (208 words), Significance (114 words), Introduction (685 words), Discussion (1406 words), 4 figures

Conflict of interest: The authors declare no conflict of interest

Author contributions:

SA & JD designed the experiment.
SA collected and analyzed the data.
SA wrote the original draft.
SA, JP, & JD conducted review and editing.

Acknowledgements:

The work was supported by a Discovery Grant from the Natural Sciences and Engineering Research Council (NSERC, RGPIN-2016-04890) to JD. Functional imaging costs were partly supported by a Platform Support Grant from Brain Canada and the Canada First Excellence Research fund (CFREF, BrainsCAN). SA was supported by a doctoral scholarship from NSERC (PGSD3-519263-2018). JP is supported by the Canada Research Chairs program.

1 Abstract

2 The integration of somatosensory signals across fingers is essential for dexterous object
3 manipulation. Previous experiments suggest that this integration occurs in neural
4 populations in the primary somatosensory cortex (S1). However, the integration process has
5 not been fully characterized, as previous studies have mainly used two-finger stimulation
6 paradigms. Here, we addressed this gap by stimulating all 31 single- and multi-finger
7 combinations. We measured population-wide activity patterns evoked during finger
8 stimulation in human S1 and primary motor cortex (M1) using 7T functional magnetic
9 resonance imaging (fMRI) in female and male participants. Using multivariate fMRI
10 analyses, we found clear evidence of unique non-linear interactions between fingers. In
11 Brodmann area (BA) 3b, interactions predominantly occurred between pairs of
12 neighbouring fingers. In BA 2, however, we found equally strong interactions between
13 spatially distant fingers, as well as interactions between finger triplets and quadruplets. We
14 additionally observed strong interactions in the hand area of M1. In both M1 and S1, these
15 non-linear interactions did not reflect a general suppression of overall activity, suggesting
16 instead that the interactions we observed reflect rich, non-linear integration of sensory
17 inputs from the fingers. We suggest that this non-linear finger integration allows for a
18 highly flexible mapping from finger sensory inputs to motor responses that facilitates
19 dexterous object manipulation.

20 **Significance statement**

21 Processing of somatosensory information in primary somatosensory cortex (S1) is
22 essential for dexterous object manipulation. To successfully handle an object, the
23 sensorimotor system needs to detect complex patterns of haptic information, which
24 requires the non-linear integration of sensory inputs across multiple fingers. Using
25 multivariate fMRI analyses, we characterized brain activity patterns evoked by stimulating
26 all single- and multi-finger combinations. We report that progressively stronger multi-
27 finger interactions emerge in posterior S1 and in the primary motor cortex (M1), with
28 interactions arising between inputs from neighbouring and spatially distant fingers. Our
29 results suggest that S1 and M1 provide the neural substrate necessary to support a flexible
30 mapping from sensory inputs to motor responses of the hand.

31 Introduction

32 When writing with a pen or manipulating a Rubik's cube in one hand, the sensorimotor
33 system needs to integrate somatosensory information from multiple fingers to estimate the
34 object's shape, position, and movement within the hand. The mechanism that underlies this
35 integration, however, remains poorly understood. We hypothesized that, in order to
36 support flexible behavioural responses to any pattern of sensory stimulation across the
37 hand, sensory inputs from neighbouring and non-neighbouring fingers need to be
38 integrated in a non-linear fashion. This non-linear code provides the neural substrate
39 necessary to detect any specific pattern of stimulation across the hand and forms the basis
40 for learning flexible mappings between sensory inputs and motor responses of the hand.

41 Stimulation to the fingers is relayed from mechanoreceptors via the cuneate nucleus to
42 the thalamus, with signals from different fingers remaining largely segregated (Florence,
43 Wall, & Kaas, 1988, 1989). Signals from different fingers begin to interact substantially only
44 in S1 and M1 (Hsieh et al., 1995). Cortical sensory processing is critical for dexterous hand
45 control, as perturbing either the transmission of somatosensory information from the hand
46 to the cortex (Moberg, 1958; Monzée, Lamarre, & Smith, 2003; Chemnitz, Dahlin, &
47 Carlsson, 2013), or lesioning S1 (Carlson, 1981; Hikosaka et al., 1985; Brochier et al., 1999)
48 grossly impairs fine manual dexterity. We refer here to S1 and M1 collectively as
49 sensorimotor cortex. In the primate brain this comprises six cytoarchitectonically distinct
50 Brodmann areas (BA): 4a, 4p, 3a, 3b, 1, and 2 (Brodmann, 1909; Powell & Mountcastle,

51 1959; Geyer et al., 1996). Inputs from the thalamic somatosensory nuclei vary across these
52 regions, with BA 3a and BA 3b receiving most of the inputs, BA 4a and BA 4p receiving a
53 substantial amount, and BA 1 and BA 2 receiving progressively fewer (Jones & Powell,
54 1970; Jones, 1975; Shanks & Powell, 1981; Darian-Smith & Darian-Smith, 1993). In
55 nonhuman primates, neurons in BA 3b have receptive fields mainly devoted to single
56 fingers, whereas in BA 1 and BA 2, receptive fields encompass multiple fingers (Hyvärinen
57 & Poranen, 1978b; Sur, 1980; Iwamura et al., 1993). Measuring the coarse spatial
58 organization for fingers in these regions with fMRI reveals comparable findings in humans,
59 with finger representations becoming more spatially overlapping in posterior subregions of
60 S1 (Krause et al., 2001; Martuzzi, et al., 2014; Besle et al., 2014). At the single-neuron level,
61 paired finger stimulation generally results in lower firing rates relative to what would be
62 expected from summing the firing rates resulting from single finger stimulation (Friedman,
63 Chen, & Roe, 2008; Lipton et al., 2010; Reed et al., 2010; Thakur, Fitzgerald, & Hsiao, 2012).
64 Together, these findings have been interpreted as evidence that inputs from multiple
65 fingers are integrated in the sensorimotor cortex (Iwamura, 1998; Yau et al., 2016).

66 Everyday object manipulation often demands the integration of information across all
67 fingers of the hand. In contrast, most previous studies have typically examined stimulation
68 of only a few pairs of fingers. Consequently, the full nature of the interactions that occur
69 between somatosensory inputs from all five fingers is not well characterized. Furthermore,
70 it is unclear whether these previously reported suppressive interactions reflect the encoding
71 of specific patterns of multi-finger stimulation (i.e., non-linear finger integration) or simply

72 divisive normalization (Carandini & Heeger, 2011; Brouwer et al., 2015), where the inputs
73 coming from individual fingers are linearly combined, but the net activity is suppressed
74 through a diffuse inhibition. Studies of finger integration in humans also share these
75 limitations (Gandevia, Burke, & McKeon, 1983; Hsieh et al., 1995; Biermann et al., 1998;
76 Ishibashi et al., 2000; Hoechstetter et al., 2001; Ruben et al., 2006).

77 Here, we addressed this gap by studying all 31 possible finger combinations by
78 simultaneously stimulating one, two, three, four, or five fingers of the right hand. We
79 measured activity patterns evoked in the hand area of the sensorimotor cortex using 7T
80 fMRI while human participants experienced passive tactile stimulation. Consistent with
81 previous work, we found progressive overlap of single finger representation in
82 sensorimotor cortex. By analyzing the multivoxel activity patterns in each subregion, we
83 also found clear evidence for progressively stronger multi-finger interactions in posterior
84 S1 and M1.

85 **Materials and Methods**

86 **Participants**

87 Ten healthy participants were recruited for the study (7 males and 3 females, mean
88 age=25.5, SD=3.24; median Edinburgh handedness score=80.0, median absolute
89 deviation=20.0). Participants completed one training session and two experimental
90 sessions. During the training session, participants were familiarized with the finger
91 stimulation task. In the two experimental sessions, participants experienced finger
92 stimulation while undergoing 7T fMRI. All participants provided informed consent before
93 the beginning of the study, and all procedures were approved by the Office for Research
94 and Ethics at the University of Western Ontario.

95 **Apparatus**

96 We used a custom-built five-finger keyboard to apply stimulation independently to
97 each of the five fingers of the right hand. Each finger was comfortably restrained above an
98 immobile key using a clamp covered with padding (Fig. 1A). The clamp prevented any
99 hand or finger movement and ensured that the passive stimulation was delivered to a
100 constant area of the fingertip. We delivered independent stimulation to each fingertip
101 using a pneumatic air piston mounted underneath each key. The pistons were driven by
102 compressed air (100 psi) delivered from outside the MRI scanning room through polyvinyl
103 tubes. The forces applied to the fingertips were monitored using force transducers
104 (Honeywell-FS series, dynamic range=0-16N, resolution<0.02N, sampling rate=200Hz), and

105 the air pressure for each piston rod was independently regulated using PID control to
106 deliver forces of ~3 Newtons to each fingertip (one participant experienced stimulation of
107 ~2N). The piston rods (diameter=3mm) deformed the skin of the fingertip. As the padding
108 prevented movement of the finger, the stimulation was predominantly tactile in that it
109 involved deformation of the skin.

110 **Task**

111 **Finger stimulation:** While lying in the scanner, participants viewed a back-projection
112 screen through a mirror mounted to the head coil. They saw five bars in the centre of the
113 screen, surrounded by a box (Fig. 1B). Each bar corresponded to one of the five fingers of
114 the right hand (left-to-right: thumb-to-little finger). All 31 possible finger combinations
115 were stimulated (5 single-finger, 10 two-finger, 10 three-finger, 5 four-finger, and 1 five-
116 finger configuration; Fig. 1C).

117 Each trial lasted 6.5s and consisted of four phases (Fig. 1B): a cue phase (0.5s), finger
118 stimulation (4s), perceptual judgement ($\leq 1.5s$), and feedback ($\geq 0.5s$). The cue phase alerted
119 participants to the start of the trial. During the cue, the outline box turned orange and the
120 words "RELAX FINGERS" were presented on screen, instructing participants to relax their
121 hand. No information was provided about which finger combination was going to be
122 stimulated, and therefore participants remained naïve about the stimulation until it
123 occurred. At the start of the stimulation phase, the words disappeared from the screen and
124 the box turned white, after which one of the 31 possible finger combinations was

125 stimulated. The stimulated force on each finger approximated a rectified sine wave,
126 gradually increasing and decreasing. Each "wave" of stimulation lasted approximately 1s,
127 and two complete waves were delivered during each trial. Across all fingers and
128 combinations, the average measured peak force was $2.67 \pm 0.17\text{N}$.

129 **Mismatch detection:** In the perceptual judgement phase of each trial, we presented a
130 visual arrangement of a specific finger combination, with the boxes corresponding to the
131 stimulated fingers turning orange (Fig. 1B). To ensure that participants remained attentive
132 during the experiment, we asked them to detect the occurrence of relatively rare (5% of
133 trials) mismatches between the visually presented and stimulated patterns (probe trials).
134 Participants were asked to detect this mismatch and indicate it by pressing their right
135 thumb (2N threshold). If the presented and stimulated pattern matched, they were
136 instructed to refrain from pressing any finger. We chose this particular task because it
137 ensured that participants remained attentive, but it did not explicitly require the integration
138 of sensory information across fingers. On the contrary, the task demanded that sensory
139 information from each finger be analyzed separately.

140 Participants had 1.5s to judge and respond. After either 1.5s elapsed (indicating a
141 match) or immediately following a thumb press (indicating a mismatch), participants were
142 provided feedback on their response by changing the colour of the finger combination
143 green (correct) or red (incorrect). The feedback was presented on-screen for $\geq 0.5\text{s}$, such
144 that the feedback and response phases together lasted 2s regardless of response type.

145 To encourage good performance, participants received points based on the
146 performance of their perceptual judgements. They were awarded 1 point for correctly
147 identifying a matching configuration, and 10 points for correctly identifying a mismatched
148 configuration. False alarms were penalized by -1 point, and misses (failing to recognize a
149 mismatch configuration) were penalized by -10 points. Points were combined across
150 imaging runs and used to calculate a financial bonus. Behavioural performance on the
151 perceptual judgement task was high (overall error rate= $1.77\pm0.40\%$) with participants being
152 well able to discriminate perceptual mismatch trials (hit rate= $86.97\pm5.09\%$, false alarm
153 rate= $1.20\pm0.21\%$, $d'=3.68\pm0.31$). Although participants tended to be conservative in their
154 response behaviour (i.e., they were somewhat biased to not report a mismatch:
155 $c=0.44\pm0.11$), this was expected because most of the trials (95%) were matches and thus
156 required participants to refrain from making a thumb press. Together, this resulted in
157 participants making a thumb press on $5.35\pm0.20\%$ of all trials.

158 **Procedure**

159 Participants completed one training session and two imaging sessions. Each session
160 was comprised of several runs. Each run contained 62 trials, with two trials for each of the
161 31 finger combinations (see Finger stimulation). 5% of these trials contained perceptual
162 mismatches (see Mismatch detection). Trials were separated by a variable inter-trial-interval
163 (ITI), drawn randomly from the set of possible ITIs {1s, 2.5s, 4s, 5.5s, 7s, 8.5s, 10s}, with the
164 probability $p=[0.37, 0.24, 0.16, 0.10, 0.06, 0.04, 0.03]$ for each ITI, respectively. Thus, shorter

165 delays occurred more often and longer delays occurred less often. The order of trials,
166 including the position of the mismatch trials, was randomized across runs and participants.

167 During training, participants performed runs of trials until they achieved an overall error
168 rate of 0% in one run. Participants completed the training session 1-2 days before the first
169 scanning session. For the imaging sessions, participants completed 11 total runs, yielding
170 682 total trials (31 combinations x 2 repeats x 11 runs). These 11 runs were split over two
171 separate scanning sessions for each participant, usually within the same week.

172 **MRI data acquisition**

173 We used high-field functional magnetic resonance imaging (fMRI, Siemens 7T
174 Magnetom with a 32-channel head coil at Western University, London, Ontario, Canada) to
175 measure the blood-oxygen-level dependent (BOLD) responses evoked in participants. Each
176 participant completed 11 runs of trials across two separate scanning days, usually with 6
177 runs on the first day and 5 runs on the second day. Each run lasted 614s. During each run,
178 410 functional images were obtained using a multiband 2D-echoplanar imaging sequence
179 (GRAPPA, in-plane acceleration factor=2, multi-band factor=3, repetition time [TR]=1500ms,
180 echo time [TE]=20ms, in-plane resolution 148 x 148 voxels). Per image, we acquired 66
181 interleaved slices (without gap) with isotropic voxel size of 1.4mm. The first 2 images in the
182 sequence were discarded to allow magnetization to reach equilibrium. To estimate
183 magnetic field inhomogeneities, we acquired a gradient echo field map at the end of the
184 scanning session on each day. Finally, a T1-weighted anatomical scan was obtained using a

185 magnetization-prepared rapid gradient echo sequence (MPRAGE) with a voxel size of
186 0.75mm isotropic (3D gradient echo sequence, TR=6000ms, 208 volumes).

187 **fMRI preprocessing and first-level analysis**

188 Functional images were first realigned to correct for head motion during the scanning
189 sessions (3 translations: x,y,z; 3 rotations: pitch, roll, yaw), aligned across sessions to the
190 first image of the first session, and co-registered to each participant's anatomical T1-image.
191 Within this process, we used B0 fieldmaps from each imaging session to correct for image
192 distortions arising from magnetic field inhomogeneities (Hutton et al., 2002). Due to the
193 relatively short TR (1.5s), no slice-timing correction was applied, and no spatial smoothing
194 or normalization to a standard template was applied.

195 The minimally preprocessed data were then analyzed using a general linear model
196 (GLM; Friston, Jezzard, & Turner, 1994) using SPM12 (filion.ucl.ac.uk/spm/) with a separate
197 regressor for each of the 31 possible finger combinations in each run. The activation
198 during stimulation was modeled using a boxcar function that spanned the stimulation
199 phase of each trial, convolved with a hemodynamic response function with a delayed onset
200 of 1.5s and a post-stimulus undershoot at 12s. Given the low error rate, all trials were
201 included in the analysis, regardless of the perceptual judgement accuracy. To capture
202 activity evoked by the thumb press during mismatch detection, we included one thumb
203 press regressor in each run which modeled all thumb responses per run (duration: 1s).
204 Because the response was always the same thumb press and occurred with roughly equal

205 probability for each finger combination, any incomplete modelling of the response-evoked
206 activity should not influence our results pertaining to the differences in activity patterns
207 between finger combinations. Finally, we included an intercept regressor for each run,
208 yielding 363 total regressors (33 regressors x 11 runs).

209 To model the long-range temporal autocorrelations in the functional timeseries, we
210 used the SPM FAST autocorrelation model. High-pass filtering was then achieved by
211 temporally pre-whitening the functional data with this temporal autocorrelation estimate.
212 This analysis yielded one beta-weight for each voxel for each of the 31 finger combinations
213 per run for each participant. Collectively, these defined the estimated activity patterns. We
214 did not further analyze the activity pattern from the thumb press regressor. From these
215 beta-weights, we calculated the average percent signal change (PSC) evoked by each finger
216 combination relative to the baseline for each voxel, yielding 31 PSC values per voxel.

217 **Surface-based analyses**

218 **Surface reconstruction:** We used Freesurfer (Fischl, Sereno, & Dale, 1999) to
219 reconstruct the cortical surface from the anatomical image of each participant, with each
220 node having a location on the white-matter/gray-matter surface and the pial surface. The
221 surfaces were then spherically registered to match a template atlas (FreeSurfer's Left-Right
222 164k node template) based on a sulcal-depth map and local curvature.

223 **Projection of activity patterns to cortical surface:** To visualize the evoked activity
224 patterns, the individual patterns were projected on the individual surface. For each surface

225 node, all voxels that lay between the white matter and the pial surface location for that
226 node were averaged. To avoid the mixing of signals between M1 and S1 across the central
227 sulcus, we excluded voxels that projected to two dis-connected groups of surface nodes
228 (one on the anterior and one on the posterior bank of the central sulcus) with the second
229 projection accounting for at least 25% of the total surface (see
230 github.com/DiedrichsenLab/surfAnalysis for details).

231 **Surface-based searchlight:** For multivariate analysis, we used a surface-based
232 searchlight approach (Oosterhof et al., 2011). For each node on the individual surface
233 reconstruction, we used a geodesic distance metric to define a circular region on the
234 surface that included the nearest 160 voxels between the pial and white/gray-matter
235 surface (average geodesic radius= $5.85 \pm 0.04\text{mm}$). The use of a geodesic metric ensured
236 that each searchlight region did not include voxels across a sulcus. The set of activity
237 patterns from these voxels were then analyzed together (see Multivariate fMRI analysis)
238 and the results were assigned to the corresponding centre node. The searchlight analysis
239 was primarily used for visualization purposes (e.g., Fig. 2C).

240 **Cross-sectional profile plots:** To create the cross-sectional surface profiles of
241 univariate and multivariate measures (e.g., Fig. 2B & D), we used the data that fell into a
242 rectangular box that spanned the sensorimotor cortex of each participant (dashed
243 rectangle in Fig. 2A). We orthogonally projected surface nodes within the rectangular box
244 onto a cross-sectional line that approximately spanned the rostral-caudal axis from BA 4a
245 to 2. Following, data from the projected nodes where then averaged within 101 equidistant

246 bins along this cross-section. Figure 2B and D show the group-averaged cross-sectional
247 profiles. As with the searchlight analysis, the cross-sectional profiles were primarily for
248 visualization purposes.

249 **Surface-based tessellation:** To conduct more computationally intensive
250 representational model comparisons (see Representational model analysis) across the
251 cortical surface, we employed a coarser alternative to the continuous surface-based
252 searchlight approach: We defined a reduced set of surface patches by tessellating the left
253 hemisphere into 1442 regular hexagonal tessels. We then sub-selected a set of tessels that
254 had enough reliable differences between stimulation conditions to allow for model-
255 comparison. Specifically, a tessel was included if the group-averaged continuous
256 searchlight result showed an average pattern dissimilarity across all activity patterns of
257 ≥ 0.005 . This criterion yielded 82 tessels that spanned the surface of sensorimotor cortex,
258 with an average of 98.93 ± 2.81 voxels per tessel.

259 **Regions of interest definition**

260 For a targeted analysis of subregions of the sensorimotor cortex, we used a
261 probabilistic cytoarchitectonic atlas projected to the cortical surface (Fischl et al., 2008) to
262 define Brodmann areas 4a, 4p, 3a, 3b, 1, and 2. Surface nodes were assigned to the region
263 that had the highest probability, and this probability needed to exceed 0.25. We further
264 restricted these regions to the hand area by excluding nodes that fell 2.5cm above and
265 2.5cm below the hand knob anatomical landmark (Yousry et al., 1997). To avoid smearing

266 activity across the central sulcus, we excluded (as in the surface projection) voxels with
267 >25% of their volume in the gray matter on the opposite side of the central sulcus. This
268 yielded 546.70 ± 35.45 voxels for BA 4a, 642.20 ± 41.99 voxels for BA 4p, 275.20 ± 10.48 voxels
269 for BA 3a, 711.00 ± 31.05 voxels for BA 3b, 602.40 ± 33.50 voxels for BA 1, and 1034.30 ± 57.80
270 voxels for BA 2.

271 **Single-finger selectivity**

272 **Voxel selection:** To quantify the selectivity of each voxel for a specific finger, we
273 considered only the activity estimates for the single-finger conditions. We selected voxels
274 from each region that showed significant modulation (relative to baseline) during any
275 single-finger stimulation, by conducting an omnibus *F*-test per voxel, retaining only voxels
276 that were significant on an $p=0.05$ level (uncorrected). This criterion selected $8.98 \pm 1.24\%$ of
277 the voxels from BA 4a (50.70 ± 8.58 voxels), $7.62 \pm 0.88\%$ from BA 4p (48.30 ± 5.60 voxels),
278 $8.19 \pm 1.23\%$ from BA 3a (22.50 ± 3.61 voxels), $14.84 \pm 2.10\%$ from BA 3b (105.60 ± 15.73
279 voxels), $16.60 \pm 2.57\%$ from BA 1 (101.50 ± 16.78 voxels), and $10.91 \pm 1.46\%$ from BA 2
280 (116.50 ± 20.91 voxels). We verified in simulations that this voxel selection approach did not
281 bias the subsequent selectivity analysis, but simply increased its power. This is because the
282 omnibus *F*-test only tests *if* a voxel is tuned to one or more fingers, whereas the selectivity
283 analysis characterizes the *shape* of the voxel's tuning to different fingers.

284 **Quantifying selectivity:** We then normalized the tuning curves (5 activity values for
285 each voxel), such that the maximal response equaled 1 and the lowest response equaled 0.
286 For the plots in Figure 3B, we grouped the voxels according to the most preferred finger.

287 Using the normalized tuning curve for each voxel, we calculated the voxel's selectivity
288 (λ) as:

$$\lambda = 1 - \frac{1}{4} \sum_i y_i$$

289 , where y_i are the normalized responses to the four "less-preferred" fingers. This yields
290 the average difference between the activity evoked by the finger that the voxel is most
291 *tuned* to (the maximal activity) and all other finger activities. Therefore, $\lambda = 1$ indicates a
292 voxel is only active during stimulation of a specific finger. Conversely, $\lambda < 1$ indicates that a
293 voxel also responds to stimulation of other fingers. For each participant, we averaged the
294 resulting selectivity coefficients across the selected voxels per region. This yielded one
295 selectivity coefficient per region per participant, which are plotted in Figure 3C.

296 **Controlling for measurement noise:** Due to measurement noise, the estimated
297 selectivity coefficients will always be <1 , even if all voxels would only respond to a single
298 finger. The level of signal-to-noise may differ across regions and participants, making it
299 inappropriate to directly compare the raw selectivity coefficients. Furthermore, even
300 completely random tuning would still result in estimated selectivity coefficients >0 . To
301 address this issue, we simulated voxel tuning curves under two different generative models.
302 First, for random tuning, we simulated voxels with tuning that was drawn from a

303 multivariate Gaussian distribution, with covariance identical to the group-averaged finger-
304 by-finger correlation matrix (Ejaz, Hamada, & Diedrichsen, 2015). Second, for highly
305 selective tuning, we simulated voxels that were selective for stimulation of a single finger
306 and remained unresponsive to all other fingers. Both simulations were scaled, so that the
307 average diagonal of the covariance matrix matched the signal strength for that region and
308 participant (σ_s^2). We then added the measurement noise, drawn from a normal distribution
309 with variance set to σ_ϵ^2 , again matched to that region and participant.

310 To estimate σ_s^2 and σ_ϵ^2 from the real data of each participant, we first vectorized the
311 matrix of mean-centred tuning curves for each run, and then calculated the average
312 covariance between these vectors across runs. An estimate of σ_ϵ^2 could then be obtained
313 via $\sigma_\epsilon^2 = \frac{\sigma_s^2}{r} - \sigma_s^2$, where r is the average Pearson's correlation between the vectorized
314 tuning curves across runs. This expression arises because we assume the noise in the real
315 data is independent (i.e., uncorrelated) across different runs, and therefore, the expected
316 value of the Pearson's correlation between vectorized tuning curves from different runs is
317 $r = \sigma_s^2 / (\sigma_s^2 + \sigma_\epsilon^2)$.

318 Using these estimates, we simulated 1000 datasets with random tuning and 1000
319 datasets with perfectly selective tuning for each region in each participant, each with the
320 same number of voxels as the real data. All data sets were simulated with 11 imaging runs.
321 As for the real data, we then applied the voxel selection to the simulated data. We
322 calculated the average selectivity across voxels in each simulated dataset and averaged the
323 selectivity coefficients across simulations. For statistical comparison of selectivity

324 coefficients across regions, the selectivity of the real data was then normalized such that a
325 selectivity of 0 reflected the expected value under random tuning and 1 reflected the
326 expected value for highly selective tuning. This normalization was done for each region and
327 participant separately and ensured that comparisons across regions were not biased by
328 differences in noise.

329 **Representational similarity analysis**

330 To test for reliable differences between fMRI activity patterns for each condition (i.e.,
331 the first-level GLM beta-weights), we used the cross-validated squared Mahalanobis
332 dissimilarity (i.e., crossnobis dissimilarity, Walther et al., 2016). Cross-validation ensures the
333 dissimilarity estimates are unbiased, such that if two patterns differ only by measurement
334 noise, the mean of the estimated dissimilarities would be zero. This also means that
335 estimates can sometimes become negative (Diedrichsen et al., 2020; Diedrichsen, Provost,
336 & Zareamoghaddam, 2016). Therefore, dissimilarities significantly larger than zero indicate
337 that two patterns are reliably distinct, and we take this as evidence that features about the
338 finger combinations are represented in the activity patterns.

339 The crossnobis dissimilarity d between the fMRI activity patterns (\mathbf{x}) for conditions i
340 and j was calculated as:

$$d_{i,j} = \frac{1}{M} \sum_m^M (\mathbf{x}_i - \mathbf{x}_j)_m^T \Sigma^{-1} (\mathbf{x}_i - \mathbf{x}_j)_{\sim m}$$

341 , where the activity patterns from run m are multiplied with the activity patterns
342 averaged over all runs except m ($\sim m$). Σ is the voxel-wise noise covariance matrix,

343 estimated from the residuals of the first-level GLM, and slightly regularized to ensure
344 invertibility. Multivariate noise-normalization removes spatially correlated noise and yields
345 generally more reliable dissimilarity estimates (Walther et al., 2016). Analyses were
346 conducted using functions from the RSA (Nili et al., 2014) MATLAB toolbox. For the
347 searchlight results (Fig. 2C & 2D), we averaged the resulting dissimilarities based on
348 whether they were between single-finger patterns, 2-finger patterns, 3-finger patterns, or
349 4-finger patterns.

350 **Representational model analysis**

351 We used representational models to infer what feature sets were present in the activity
352 patterns from each region. A representational model characterizes the tuning curves of a
353 group of voxels or neurons. In the sense we are using it here, it specifies a probability
354 distribution over all possible tuning curves (Diedrichsen & Kriegeskorte, 2017). Here, we
355 used an encoding-style approach (Naselaris et al., 2011) to specify and evaluate
356 representational models that predicted activity patterns for all finger combinations using
357 various feature sets. Models were fit and evaluated using the PCM toolbox (Diedrichsen,
358 Yokoi, & Arbuckle, 2018), using cross-validation across imaging runs for each region in
359 every participant.

360 **Linear Model:** The linear model predicted that activity patterns evoked during multi-
361 finger stimulation were the sum of the constituent single-finger patterns:

$$\hat{Y}_{lin} = M_{lin}U_{sf}$$

362 , where \hat{Y}_{lin} are the [31 x P voxels] predicted activity patterns, U_{sf} is a [5 features x P
363 voxels] matrix of single-finger feature patterns, and M_{lin} is a [31 combinations x 5 features]
364 indicator matrix denoting which finger(s) are in each of the combinations. To complete the
365 representational model, we also specified that the single-finger features had a second-
366 moment matrix (co-variance matrix without subtraction of the mean across voxels) of G_{lin} .
367 The second moment matrix of finger-related patterns is highly invariant across individuals,
368 reflecting the high correlations of patterns from neighbouring fingers, and the low
369 correlation of the pattern of the thumb with the other fingers (Ejaz et al., 2015; Arbuckle et
370 al., 2020). We determined the exact form of the matrix for each region separately, using
371 the group-averaged second moment matrix \bar{G} from the region under analysis. Specifically,
372 we determined the second moment matrix for the single-finger patterns that would best
373 approximate the overall second moment matrix $G_{lin} = M_{lin}^+ \bar{G} M_{lin}^{+T}$, where M_{lin}^+ is the Moore-
374 Penrose pseudoinverse.

375 **Multi-finger interaction models:** We also constructed 3 multi-finger interaction
376 models. Like the linear model, these models assumed that the multi-finger patterns were
377 the sum of the constituent single finger patterns, but also included specific interaction
378 effects between specific fingers. These models took the same general form as the linear
379 model above. For the 2-finger interaction model, we included 10 terms indicating the
380 presence of a specific pair of fingers (i.e. when the pair of fingers was pressed, the
381 regressor was 1 and 0 otherwise), in addition to the 5 model features for the individual
382 fingers. In the 3-finger interaction model, we additionally added 10 regressors indicating

383 the presence of each unique 3-finger combination. Finally, the 4-finger model included, in
384 addition to the 3-, 2-, and 1-finger terms, the five possible 4-finger interactions, resulting
385 in 30 model features overall. For each of the models, the second-moment matrix for the
386 feature patterns U was estimated from the group-averaged second-moment matrix as for
387 the linear model.

388 **Adjacent and non-adjacent 2-finger interaction models:** To test the strength of
389 finger interactions between adjacent and non-adjacent finger pairs, we created two
390 modified versions of the 2-finger interaction model. In the first version, we only included
391 the 4 adjacent finger-pairs as interaction terms. In the second version we included only the
392 6 non-adjacent finger pairs.

393 **Linear-nonlinear model:** The linear-nonlinear model predicted that activity patterns for
394 single-fingers combined linearly when multiple fingers were stimulated, but that the overall
395 activity was compressed by a unknown, non-linear function $f, \hat{Y}_{lnl} = f(M_{lin}U_{sf})$. Such a non-
396 linearity could arise from a global divisive normalization of neural activity in the region, or
397 from non-linearities in the relationship between neural activity and the BOLD signal. To
398 approximate any form of such compressive non-linearity, we created a model, based on
399 the linear model, that allowed for flexible scaling of the predicted multi-finger patterns. All
400 predicted patterns that included the same number of stimulated fingers were scaled by a
401 common factor. These scaling factors, as well as the single-finger feature patterns U_{sf} , were
402 estimated from the training data.

403 **Null-model:** As a baseline for model comparison, we defined a null-model that
404 predicted overall activity scaled with the number of fingers stimulated, but that the
405 patterns lacked finger-specificity. Under this model, the predicted patterns were derived
406 from the average activity patterns for the single-finger, 2-finger, 3-finger, 4-finger, and 5-
407 finger combinations, respectively. For example, the predicted single-finger patterns was the
408 average pattern across the five single-finger conditions from the training data.

409 **Noise-ceiling model:** To provide an estimate of how much systematic variation could
410 be explained in the data given measurement noise, we included a "noise-ceiling" model.
411 The predictions under the noise-ceiling model were simply the 31 activity patterns from
412 the training data. Note that this fully saturated model differs from the 4-finger interaction
413 model only by the addition of a single model term that models the specific non-linearities
414 arising during the stimulation of all 5 fingers. The second-moment matrix for this model
415 was set to the observed group-averaged estimate \bar{G} for the region under analysis.

416 **Model fitting:** We fit and evaluated the different models within each participant, using
417 a leave-one-run-out cross-validation procedure. For each cross-validation fold, the training
418 data were the activity patterns from all imaging runs except one, and the test data were
419 the activity patterns from the left-out run.

420 For a representational model with the assumption that both noise and signal have
421 multivariate Gaussian distribution (Diedrichsen & Kriegeskorte, 2017), the feature patterns
422 for each model can be estimated from the training data Y_{train} as:

$$U = (X^T X + G^{-1} s^{-1} \sigma_\epsilon^2)^{-1} X^T Y_{train}$$

423 , where X is a model-specific design matrix that denoted which feature(s) were present
424 in each of the rows (activity patterns) in Y_{train} , G is the model-dependent second-moment
425 matrix as specified above, s indicates the strength of the signal in Y_{train} , and σ_ϵ^2 is the
426 variance of the random run-by-run noise. Note that this estimation takes the form of linear
427 regression with Tikhonov regularization. The strength of the regularization to the model
428 prior was determined by $s^{-1}\sigma_\epsilon^2$. For each cross-validation fold, we derived the maximum-
429 likelihood estimate of s and σ_ϵ^2 using the PCM toolbox. For the linear-nonlinear model, we
430 additionally fitted the scaling parameters by minimizing the residual sums-of-squares of
431 the model predicted patterns to the training data.

432 **Model evaluation:** The estimated feature patterns (U) were then used to predict
433 activity patterns under the corresponding model. We compared the predicted 31 condition
434 patterns with the left-out test data. The model fits were evaluated using Pearson's
435 correlation. For this, the predicted and test patterns were first mean-centred (per voxel),
436 then correlated across all voxels and conditions within each cross-validation fold. We
437 averaged the correlations across cross-validation folds to yield a single estimate of model
438 performance per participant per region. We preferred Pearson's correlation as our
439 evaluation metric over the coefficient of determination, as it is less dependent on the exact
440 choice of regularization coefficient (Diedrichsen & Kriegeskorte, 2017), and therefore
441 provides a more robust evaluation.

442 Finally, the model fits were normalized between 0 and 1, using the fits of the null and
443 noise-ceiling models. This normalization approach was necessary because, as illustrated by

444 the fits of the noise ceiling models, measurement noise varied across regions (raw
445 Pearson's r in BA 4a=0.054±0.0063, BA 4p=0.054±0.0058, BA 3a=0.074±0.010, BA
446 3b=0.116±0.013, BA 1=0.074±0.011, BA 2=0.038±0.005). Normalization of the model fits
447 enabled us to meaningfully compare fits across regions with varying levels of measurement
448 noise. Normalized fits >0 indicated that the model captured more information than the
449 simple scaling of overall activity (null model), and fits <1 indicated that there was
450 structured variance in the activity patterns that remained unaccounted for in the model(s).
451 The normalization of model fits was done for each region and participant separately.

452 **Experimental design and statistical analyses**

453 All statistical tests were performed in MATLAB R2019a (Mathworks, Inc.). We set the
454 significance level in our analyses to $p=0.05$. When a test involved multiple comparisons
455 without any specified *a priori* hypotheses, we adjusted the significance level by dividing by
456 the number of comparisons (i.e., Bonferroni correction). For clarity, we report uncorrected
457 p -values in the text. The Bonferroni-corrected statistical threshold is reported as an α -value
458 when appropriate. In cases where we had *a priori* hypotheses, we did not correct for
459 multiple comparisons (i.e., replicating single-finger pattern overlap; Fig. 3C). To compare
460 evoked activity, dissimilarities, or normalized model fits across regions, we used within-
461 participant repeated measures ANOVAs. We used two-sided paired t-tests to compare the
462 model fits to the fit of the noise-ceiling in each region. If the model fit did not differ
463 significantly from the fit of the noise-ceiling model, we considered the model to be as

464 good as the noise-ceiling. Therefore, to remain conservative, we evaluated uncorrected p -
465 values and did not correct for multiple comparisons for this analysis, as this correction
466 would lower the bar for what would be considered a "good-fitting" model.

467 **Data and Code Accessibility**

468 The analyses reported in this paper relied on code from the Representational Similarity
469 Analysis (github.com/rsagroup/rsatoolbox_matlab) and Pattern Component Modeling
470 (github.com/jdiedrichsen/pcm_toolbox) MATLAB toolboxes. The pre-processed data and
471 code necessary to reproduce analyses and plots are available on github
472 (github.com/saarbuckle/finger-sensory-integration).

473 **Results**

474 **Finger stimulation evokes broadly distributed activity in sensorimotor
475 cortex**

476 Using high-resolution 7T fMRI, we measured the activity patterns evoked by passive
477 finger stimulation in the brains of 10 human participants. Stimulation was delivered
478 independently to each fingertip of the right hand by indenting the skin with a small rod
479 pushed by a pneumatic piston. We tested the entire set of 31 single- and multi-finger
480 combinations. To keep participants engaged during the experiment, they were instructed to
481 detect rare mismatches between the stimulated combination and a visual probe presented
482 after finger stimulation (see Methods).

483 Figure 2A shows the group-average percent signal change (relative to rest) during
484 right-hand finger stimulation on a flattened surface view of the cortical hand regions in S1
485 and M1 of the left hemisphere. During single-finger stimulation, evoked activity was low,
486 but as more fingers were stimulated, we observed an increase in overall activity across
487 subregions of the sensorimotor cortex. To statistically evaluate activity, we subdivided the
488 hand region into six anatomically defined Brodmann areas using a cytoarchitectonic atlas
489 (Fischl et al., 2008), spanning from BA 4a to BA 2 (see Methods). In each BA subregion,
490 activity increased when more fingers were stimulated (all $F_{(4,36)} \geq 4.730$, all $p \leq 0.0036$; see Fig.
491 2B).

492 This activity increase does not provide a detailed view of how sensory information from
493 different fingers is integrated in the human sensorimotor cortex. As a starting point to
494 address this question, we quantified how dissimilar the local single-finger activity patterns
495 were from each other. We used a crossvalidated estimate of the dissimilarity measure
496 (crossnobis, see Methods), such that a value of zero indicated that patterns only differed by
497 noise, and dissimilarity values greater than zero indicated that the patterns were distinct.
498 The average dissimilarities showed that single-finger stimulation evoked distinct finger
499 patterns in all subregions (Fig. 2C). Indeed, all considered BA regions showed highly
500 significant finger-specific pattern differences (one-sided t-test >0 : all $t_9 \geq 3.012$, all $p \leq 0.0073$,
501 Bonferroni corrected α -value=0.0083), which suggests that each region received
502 information about the stimulated fingers. Dissimilarities between all 2-, 3-, and 4-finger
503 combinations showed a similar spatial distribution, although the overall magnitude of the
504 dissimilarities was reduced compared to the single-finger patterns (Fig. 2D). This finding is
505 expected because multi-finger combinations also share an increasing number of fingers.

506 **Increasing overlap of single-finger patterns in sensorimotor cortex**

507 Based on previous electrophysiological (Hyvärinen & Poranen, 1978b; Sur, 1980;
508 Iwamura et al., 1993) and fMRI (Martuzzi et al., 2014; Besle et al., 2014) results, we would
509 expect to find relatively focal single-finger activation in BA 3b, with more overlap between
510 fingers in other parts of the sensorimotor cortex. This seemed to be the case as shown in
511 the single-finger patterns for two exemplary participants (Fig. 3A). Each finger activated a

512 quite distinct region of BA 3b and BA 3a. In contrast, the spatial patterns for each finger in
513 BA 1 and BA 2, as well as in M1 (BA 4a and BA 4p) were more complex and involved
514 multiple “hot spots” per finger, with substantial overlap between fingers.

515 We quantified this observation by computing a measure of finger-selectivity for each
516 voxel. We selected voxels from each region that were significantly responsive to stimulation
517 of any individual finger (see Methods), and scaled the responses of these voxels, such that
518 the activity associated with the finger that evoked the largest positive response (i.e., the
519 most-preferred finger) equaled 1, and the activity associated with the finger that evoked
520 the smallest response (i.e., the least-preferred finger) equaled 0. If the voxel was only tuned
521 to one finger, all non-preferred fingers would have a value of zero. The average scaled
522 responses for the 4 non-preferred fingers therefore can be used as a measure of the
523 selectivity of that voxel (Fig. 3B). To then define a selectivity index, we subtracted the
524 averaged scaled responses for the 4 non-preferred fingers from 1, such that 1 indicates
525 maximal selectivity, and 0 equal activation for all fingers. We averaged the selectivity
526 coefficients across voxels per participant in each region.

527 Before comparing the selectivity coefficients across regions, we needed to address one
528 last problem – namely, regions with less reliable data could appear to be more broadly
529 tuned to multiple fingers simply because higher measurement noise makes the tuning less
530 clear. This is a concern because the strength of single-finger representations, as measured
531 in the average pattern dissimilarities, varied across regions (Fig. 2D). Previous imaging work
532 (Martuzzi et al., 2014; Besle et al., 2014) has not accounted for this potential confound.

533 Here we addressed this issue by computing the expected selectivity index for random
534 tuning and for highly selective tuning, given the signal reliability in each region and each
535 participant (see Methods). We then normalized the measured selectivity coefficients for
536 each participant and region separately, with 0 indicating random tuning and 1 indicating
537 highly selective tuning for a single finger only.

538 After carefully controlling for signal reliability across regions, we confirmed that voxels
539 in BA 3b showed strong selectivity for single fingers (Fig. 3C), significantly more than
540 expected from random tuning (one-sided t-test >0 : $t_9=8.329$, $p=8.01e-6$). In comparison,
541 more posterior subregions of S1 were more broadly tuned, indicated by significantly lower
542 selectivity indices compared to BA 3b (BA 1: $t_9=3.166$, $p=0.0057$, BA 2: $t_9=4.292$,
543 $p=0.0010$). Indeed, in BA 2, the finger selectivity coefficients did not differ from what would
544 be expected assuming random tuning curves ($t_9=-0.029$, $p=0.5112$). Moving anterior
545 relative to BA 3b, voxels were less selective in BA 3a ($t_9=3.900$, $p=0.0018$).

546 Selectivity indices in M1 were significantly lower than in BA 3b, for both posterior (BA
547 4p, $t_9=6.944$, $p=3.366e-5$) and anterior portions (BA 4a, $t_9=4.177$, $p=0.0012$). Rathelot and
548 Strick (2009) proposed that “new M1” (BA 4p) is more essential for individuated finger
549 movements than “old M1” (BA 4a), from which one may predict that BA 4p should show
550 more selective single-finger representation. To test this prediction, we contrasted BA 4p
551 and BA 4a, which may approximate old and new M1, respectively. Contrary to this
552 prediction we found no difference in the average selectivity coefficients between these
553 regions ($t_9=-0.991$, $p=0.8262$). Taken together, however, our analyses confirm the idea that

554 sensory information from individual fingers is spatially quite segregated in BA 3b, but then
555 continuously intermixes when moving more anterior or posterior in the sensorimotor
556 cortex.

557 **Interactions between finger activity patterns explain spatial complexity of**
558 **multi-finger patterns**

559 Having established that somatosensory inputs from different fingers heavily overlap in
560 regions of the sensorimotor cortex, we then asked how somatosensory inputs are
561 integrated across fingers. As a first step, we inspected the spatial activity patterns evoked
562 during multi-finger stimulation. Figure 4A shows the activity patterns from two exemplary
563 participants during stimulation of the index finger, the little finger, or during stimulation of
564 both fingers. The spatial patterns evoked by stimulating each finger had a relatively focal
565 activation point in BA 3b. For the combined stimulation, we can see two areas of activation,
566 one corresponding to the region active for the index finger, and the other corresponding
567 to the region active during for the little finger. This suggests that the representation of
568 inputs from multiple fingers in BA 3b may be linear, simply reflecting the superposition of
569 activity caused by the stimulation of the individual fingers. We would expect such linearity
570 if the inputs from different fingers do not interact with each other.

571 In contrast, the multi-finger spatial pattern in BA 1 and BA 2 appeared more complex,
572 with clusters of activity emerging during simultaneous stimulation that were not present
573 when either finger was stimulated individually. Given that the neural populations

574 representing each finger appeared to be more overlapping in these same regions, the
575 complexity of the spatial patterns suggests the presence of an interaction between fingers.

576 To test this idea formally, we fit a series of representational models to the activity
577 patterns in each participant and region. These encoding-style models were fit to the
578 activity patterns across all voxels in a region during single- and multi-finger stimulation,
579 and then evaluated by their ability to predict multi-voxel activity patterns measured during
580 an independent test run (see Methods). To meaningfully compare model fits across regions
581 with different signal-to-noise levels, we normalized them to the performance of a null
582 model and a noise-ceiling model. The null model predicted that the overall activity would
583 increase when more fingers are stimulated, but that the activity patterns themselves would
584 not differ between finger combinations. The noise-ceiling model was fit by estimating a
585 unique pattern for each finger combination from the data (i.e., the model allowed for any
586 arbitrary non-linearity). The model fits were then normalised between the null model (0)
587 and noise-ceiling model (1), to express how much of the replicable finger-specific variation
588 in the activity patterns each model could explain.

589 Based on the observations in BA 3b, we first examined to what degree multi-finger
590 patterns were simply the sum of the constituent single-finger patterns. The predictive
591 performance of this linear model was significantly better than that of the null model across
592 the sensorimotor cortex (region x model ANOVA, main effect of model: $F_{(1,9)}=590.662$,
593 $p=1.618e-9$; see Fig. 4B), indicating that the linear model captured some reliable aspects of
594 the spatial activity patterns. Furthermore, the normalized linear model fit varied across

595 regions (region x model ANOVA, interaction effect: $F_{(5,45)}=7.308$, $p=4.385e-5$). The best fit
596 was observed in BA 3b, with significantly lower fits in all other regions (all $t_g \geq 4.139$, all
597 $p \leq 0.0025$, evaluated at a Bonferroni corrected α -value=0.01) except BA 3a ($t_g=2.822$,
598 $p=0.0200$), where the difference was not significant after correction. Importantly, in all
599 regions the linear model predicted the data significantly worse than the noise-ceiling
600 model (all $t_g \geq 5.318$, all $p \leq 0.0005$), indicating that there were systematic non-linearities in
601 the multi-finger activity patterns that could not be explained by the linear model.

602 To visualize more generally how the linear model fit across the sensorimotor cortex in
603 a region-blind manner, we applied the same model fitting to data from regularly
604 tessellated regions (Fig. 4C, see Methods). This yielded similar results, with good fits in BA
605 3b and increasing non-linearities in regions anterior and posterior to it (denoted by the
606 drop in performance of the linear model).

607 We then considered the possibility that non-linearities in how the activity patterns for
608 single fingers combine would arise from the interaction of pairs of fingers, perhaps via
609 local surround-inhibition or divisive normalization between two finger representations.
610 Therefore, we created a two-finger interaction model, which explained all patterns as the
611 sum of the component single-finger patterns, as well as their two-finger interactions (see
612 Methods). Across all regions, this two-finger interaction model predicted left-out data
613 significantly better than the linear model (region x model ANOVA, main effect of model:
614 $F_{(1,9)}=209.851$, $p=1.526e-7$).

615 The amount of variance explained by these two-finger interactions, however, differed
616 across regions (Fig. 4D). While the two-finger interactions lead to a small gain in predictive
617 performance in BA 3b ($8.44\pm0.83\%$), the gain was over four times larger in BA 2
618 ($37.37\pm4.41\%$). Indeed, the region x model interaction effect was highly significant
619 ($F_{(5,45)}=9.753$, $p=2.320\text{e-}6$). This indicates that a larger proportion of the pattern variance
620 could be explained in regions outside of BA 3b when including interaction effects between
621 pairs of fingers.

622 **Interactions do not only arise between adjacent fingers**

623 Do the non-linear interactions between fingers described above arise mostly between
624 adjacent fingers or do interactions also arise between spatially distant fingers of the hand?
625 Previous work has shown that stimulating adjacent fingers leads to lower activity compared
626 to non-adjacent fingers, which has been interpreted as evidence that adjacent fingers
627 interact more than non-adjacent fingers (Biermann et al., 1998; Friedman et al., 2008; Hsieh
628 et al., 1995; Ishibashi et al., 2000; Lipton et al., 2010). However, whether adjacent finger
629 interactions are stronger across all regions of the sensorimotor cortex is not known. We
630 investigated this by fitting two variants of the full two-finger interaction model, either
631 including only the interaction terms for either adjacent or non-adjacent finger-pairs. Using
632 only the non-adjacent pairs resulted in significantly lower model performance in all regions
633 compared to using all finger-pairs (all $t_9\leq-5.609$, all $p\leq0.0003$; see Fig. 4F). When we used
634 the adjacent finger pairs, the model performance was not significantly reduced in BA 4p

635 ($t_g=-0.605$, $p=0.5600$), BA 4a ($t_g=-2.793$, $p=0.0210$), and BA 3a ($t_g=-1.318$, $p=0.2199$) when
636 correcting for multiple comparisons (α -value=0.0083). In contrast, the fits in BA 3b, BA 1,
637 and BA 2 were significantly lower (all $t_g \leq -4.611$, all $p \leq 0.0013$). Taken together, this
638 suggests that in posterior regions of the sensorimotor cortex, interactions between both
639 adjacent and non-adjacent finger-pairs were important in explaining the multi-finger
640 activity patterns. Furthermore, a significant region x model interaction ($F_{(5,45)}=3.199$,
641 $p=0.0148$) indicated that the effect of finger adjacency differed across regions. In BA 2, the
642 predictive power of adjacent or non-adjacent interactions was comparable (two-sided
643 paired t-test: $t_g=-1.403$, $p=0.1941$), whereas non-adjacent interactions were significantly
644 less important in all other subregions (all $t_g \leq -3.090$, all $p \leq 0.0130$). This suggests that BA 2
645 shows strong interactions between finger-pairs irrespective of finger adjacency.

646 **Complexity of finger interactions increases along sensorimotor cortex**

647 Thus far, we have demonstrated that population activity across sensorimotor cortex
648 strongly represents two-finger interactions. However, in order to provide the neural
649 substrate necessary to skillfully manipulate an object held in the entire hand, the
650 sensorimotor system needs to be able to detect specific patterns of stimulation across all
651 fingers. Therefore, we should find evidence for integration of information across more than
652 two fingers.

653 In BA 3b and BA 3a, the two-finger interaction model provided a good fit to the multi-
654 finger activity patterns. In these regions, the model performance of the two-finger

655 interaction model was very close to the noise-ceiling model, accounting for $98.42 \pm 0.38\%$
656 and $95.37 \pm 2.40\%$ of the reliable pattern variance, respectively. While a small significant
657 difference remained in BA 3b (two-sided paired t-test: $t_9=4.162$, $p=0.0024$), the two-finger
658 interaction model explained the activity patterns as well as the noise-ceiling model in BA
659 3a ($t_9=1.916$, $p=0.0877$). Thus, neural populations in BA 3b and BA 3a do not appear to
660 provide a unique, and hence linearly separable, representation of all possible multi-finger
661 combinations.

662 In contrast, the predictive performance of the two-finger interaction model was still
663 lower than the noise-ceiling in the other regions (all $t_9 \geq 3.142$, all $p \leq 0.0119$; see Fig. 4E).
664 We therefore considered the interactions of three fingers in our models (see Methods). By
665 including three-finger interactions, we were able to explain the activity patterns as well as
666 the noise-ceiling model in BA 4a ($t_9=2.183$, $p=0.0569$). In BA 4p, BA 1, and BA 2, however,
667 performance was still significantly lower than the noise-ceiling (all $t_9 \geq 2.731$, $p \leq 0.0232$).
668 Only after including four-finger interactions were we able to fully explain the activity
669 patterns in these remaining regions (all $t_9 \leq 2.154$, $p \geq 0.0597$). This suggests that the
670 interactions in the most anterior and posterior regions of the sensorimotor cortex are more
671 complex, involving non-linear interactions between three or more fingers. Therefore, our
672 results appear to indicate that BA 1, BA 2, and also BA 4 integrate sensory information
673 arriving from multiple fingers to create a unique representation of specific patterns of
674 multi-finger stimulation.

675 **Finger interactions do not reflect a general suppression of activity**

676 There is, however, an alternative and relatively simple mechanism that could give rise
677 to the poor performance of the linear model in subregions of the sensorimotor cortex.
678 Specifically, it may be the case that the single-finger activity patterns combine linearly, but
679 that the overall activity in each region is scaled in a non-linear fashion. Such non-linear
680 scaling could arise from divisive normalization of the overall activity within the region, or
681 from non-linearities between neural activity and the BOLD signal.

682 To test this, we expanded the linear model to allow for non-linear scaling of overall
683 activity (see Methods). Indeed, this linear-nonlinear model provided a significantly better fit
684 than the original linear model in all BA regions (two-sided paired t-test: all $t_9 \geq 6.105$, all
685 $p \leq 0.0002$; see Fig. 4B). This alone should not be too surprising, given that the average
686 activity did not scale linearly with the number of fingers stimulated (Fig. 2B). Importantly,
687 however, the predictive performance of the two-finger interaction model remained
688 significantly better than that of the linear-nonlinear model in BA 3a, BA 3b, BA 1, and BA 4
689 (all $t_9 \geq 3.395$, all $p \leq 0.0079$). Although this difference was not significant in BA 2 after
690 applying Bonferroni correction for multiple comparisons ($t_9 = 3.291$, $p = 0.0094$, α -
691 value = 0.0083), the two-finger interaction model still accounted for $15.23 \pm 4.63\%$ more
692 pattern variance in this region. Furthermore, compared to the higher-order interaction
693 models, the linear-nonlinear model performed substantially worse in BA 2 (vs. three-finger:
694 $t_9 = -2.837$, $p = 0.0195$; vs. four-finger: $t_9 = -3.715$, $p = 0.0048$), and more generally across the
695 sensorimotor cortex (Fig. 4B). Therefore, the non-linearities captured by our multi-finger

696 interaction models likely reflect complex interactions that arise between specific sets of
697 finger patterns, rather than simply reflecting a general non-linear scaling of activity across
698 the region.

699 Discussion

700 In this study, we investigated how somatosensory information coming from the fingers
701 is integrated in different areas of the sensorimotor cortex. We hypothesized that to guide
702 skillful object manipulation, the sensorimotor system needs to be able to detect relatively
703 arbitrary combinations of sensory inputs across fingers, requiring non-linear integration of
704 any pair, triplet, and quadruplet of fingers. We reported that voxels in BA 3b tend to be
705 selectively tuned to the inputs from a single finger, whereas regions anterior and posterior
706 show less finger-specificity, even after we controlled for differences in signal to noise. In
707 previous work, this broader tuning to multiple fingers has often been interpreted as
708 evidence for finger integration (Iwamura et al., 1993; Martuzzi et al., 2014). However, spatial
709 overlap itself only suggests that individual fingers are represented in overlapping neural
710 populations— it does not necessarily mean that information from different fingers is
711 integrated. By using the full set of multi-finger combinations and representational model
712 analyses, we could show that the multi-finger patterns could not be explained by a simple
713 linear combination of the single-finger patterns. Rather, most regions showed clear non-
714 linearities, which not only reflected interactions between pairs of finger-pairs, but by any
715 combination of multiple fingers.

716 An important strength of our experimental design was that it allowed us to test
717 whether the observed non-linearities really reflected integration of information across the
718 fingers. Alternatively, a relatively simple explanation for our results is that the activity

719 patterns caused by single finger stimulations are simply summed but that the overall
720 activity is then suppressed in a non-linear fashion. Previous studies have been unable to
721 distinguish between these two explanations, as they used very few multi-finger
722 combinations, making it difficult to dissociate global non-linear activity suppression from
723 unique non-linear interactions (Gandevia et al., 1983; Hsieh et al., 1995; Biermann et al.,
724 1998; Ishibashi et al., 2000; Hoechstetter et al., 2001; Ruben et al., 2006; Lipton et al., 2010;
725 Brouwer et al., 2015). Having stimulated all possible multi-finger combinations, we had
726 sufficient leverage to distinguish between these two possibilities and were able to rule out
727 simple global suppression. That is, the interactions we report in this paper likely reflect rich,
728 non-linear integration of sensory inputs from the fingers.

729 The fit of the linear combination model was greatest in BA 3b, where neurons have
730 receptive fields that are largely restricted to single fingers (Sur, 1980; Iwamura et al., 1993)
731 and preferentially code for tactile features that can be extracted from local spatial regions
732 such as stimulus edge orientation (Hyvärinen & Poranen, 1978a; Bensmaia et al., 2008).
733 However, this is not to say that multi-finger integration was entirely absent in BA 3b.
734 Indeed, consistent with previous work (Reed et al., 2008, 2010; Lipton et al., 2010; Thakur et
735 al., 2012), we found significant finger-pair integration in BA 3b. Interactions were stronger
736 between adjacent fingers, indicating that the majority of integration that occurs in BA 3b is
737 across spatially close distances, as previously reported (Reed et al., 2008).

738 Moving posterior from BA 3b to BA 2, we observed progressively more complex multi-
739 finger interactions, with evidence for non-linear interactions of all possible multi-finger

740 combinations in BA 2. This complexity matches the changes in tactile feature preference of
741 individual neurons, shifting from local tactile features like edge orientation (Bensmaia et al.,
742 2008) to higher-order features that span multiple fingers like object curvature (Yau, Connor,
743 & Hsiao, 2013). The interactions also occurred for finger pairs of increasing spatial distance.
744 Indeed, the interactions between adjacent and non-adjacent fingers were equally strong in
745 BA 2. Such broad spatial integration is important for extracting spatially invariant higher-
746 order tactile features of an object (Yau et al., 2016). Together, these observations provide
747 empirical support for the hypothesis that tactile inputs from the hand are progressively
748 elaborated along the sensory cortical pathway (Hyvärinen & Poranen, 1978b; Phillips,
749 Johnson, & Hsiao, 1988; Iwamura, 1998).

750 We also examined sensory processing in the hand area of M1, which has commonly
751 been ignored in previous work. Although BA 4 is traditionally viewed as a motor area, it
752 receives substantial inputs from the somatosensory thalamus (Jones, 1975; Darian-Smith &
753 Darian-Smith, 1993) and from various areas of S1 (Ghosh, Brinkman, & Porter, 1987).
754 Therefore, neural populations in this region may also be involved in integrating tactile
755 inputs from the fingers, perhaps for rapid behavioural responses to object displacements
756 (Crevecoeur et al., 2017; Hernandez-Castillo et al., 2020). Our results demonstrate that there
757 were finger interactions in BA 4, and the strength of these interactions were comparable to
758 those in BA 2. However, it is not clear whether these interactions arose specifically within
759 BA 4 or reflect inputs from BA1 or BA 2

760 What benefit does non-linear integration of information across fingers provide? From
761 an ethological standpoint, non-linear finger integration allows for a more flexible mapping
762 between sensory inputs and motor responses. For example, consider the scenario where
763 you are holding a cup in your hand. Any movement of the cup across your fingers, be it
764 slipping downward out of your hand or rotating outward out of your hand, needs to be
765 countered with an increase in grip force if the goal is to stabilize the cup in your grasp
766 (Cole & Abbs, 1988). However, the appropriate response at more proximal muscles will be
767 quite different in these circumstances. Downward movement of the cup will largely require
768 activation of muscles that radially deviate the wrist and flex the elbow whereas outward
769 cup rotation will largely require activation of muscles that deviate the wrist but not flex the
770 elbow. In general, the appropriate muscle recruitment pattern cannot be determined by a
771 linear readout of inputs from each individual finger, since this could produce unnecessary
772 or even counterproductive responses. Only non-linear integration of the slip signals would
773 allow the mapping of these different patterns of sensory inputs to the appropriate patterns
774 of muscle recruitment.

775 Our results are in agreement with recent evidence from multi-whisker stimulation
776 studies in rodents, where specific combinations across whiskers are uniquely represented
777 by neural populations in the rodent barrel cortex (Laboy-Juárez et al., 2019; Lyall et al.,
778 2021). Like the human hand, the rodent whisker system has evolved to support complex
779 spatial-temporal interactions with the environment. Together with our current results, this

780 suggests that non-linear integration between somatosensory inputs occurs when the
781 detection of complex sensory patterns is ethologically significant.

782 In our experiment, we required participants to remain attentive to the finger
783 stimulation. Processes of selective attention have been shown to modulate neural firing
784 rates in response to finger stimulation (Hsiao, O'Shaughnessy, & Johnson, 1993). To what
785 degree are our findings caused by raw sensory input, and to what degree did our specific
786 mismatch detection task influence somatosensory processing? Although our task required
787 the comparison of the pattern of stimulation across fingers to a visual stimulus, the visual
788 stimulus was only presented after the somatosensory stimulation. At the moment of finger
789 stimulation, participants had no expectation as to which finger combination would be
790 stimulated. Therefore, the initial and dominant response observed in the fMRI data should
791 reflect bottom-up somatosensory processing. More importantly, the mismatch task did not
792 require integration of sensory information across fingers. Accurate performance could be
793 achieved by simply judging sensory information from each finger in an independent
794 manner. Therefore, if our mismatch task did induce any bias in the observed finger
795 representations, the bias is more likely to be towards an independent representation of
796 finger-specific inputs.

797 In general, it is very likely that task demands will influence how sensory information
798 from the hand is processed (to some degree). Indeed, neural populations in S1 are
799 modulated by inputs from M1 (Goldring et al., 2014), and the neural state of S1 is strongly
800 influenced by the planning of upcoming actions (Ariani, Pruszynski, & Diedrichsen, 2022;

801 Gale, Flanagan, & Gallivan, 2021). Such modulation is important, as the processing
802 requirements of somatosensory information depends on the task at hand. For example, the
803 reaction to object slip depends not only on the direction of the slipping object (Häger-
804 Ross, Cole, & Johansson, 1996), but also on the perceived physical properties of the object
805 (i.e., how “object-like” the simulation is, Ohki, Edin, & Johansson, 2002) and the behavioural
806 goal (Hernandez-Castillo et al., 2020). We may therefore expect that, in order to provide
807 support for flexible sensory-motor mapping, the way that information is integrated across
808 fingers changes with behavioral context. Thus, the next challenge is to probe how such
809 top-down influences alter the integration of somatosensory inputs across fingers.

810 References

- 811 Arbuckle, S. A., Weiler, J., Kirk, E. A., Rice, C. L., Schieber, M., Pruszynski, J. A., ... Diedrichsen, J.
812 (2020). Structure of Population Activity in Primary Motor Cortex for Single Finger Flexion and
813 Extension. *The Journal of Neuroscience: The Official Journal of the Society for Neuroscience*,
814 40(48), 9210–9223.
- 815 Ariani, G., Andrew Pruszynski, J., & Diedrichsen, J. (2022). Motor planning brings human primary
816 somatosensory cortex into action-specific preparatory states. *eLife*. doi:10.7554/eLife.69517
- 817 Bensmaia, S. J., Denchev, P. V., Dammann, J. F., 3rd, Craig, J. C., & Hsiao, S. S. (2008). The
818 representation of stimulus orientation in the early stages of somatosensory processing. *The
819 Journal of Neuroscience: The Official Journal of the Society for Neuroscience*, 28(3), 776–786.
- 820 Besle, J., Sánchez-Panchuelo, R.-M., Bowtell, R., Francis, S., & Schluppeck, D. (2014). Event-related
821 fMRI at 7T reveals overlapping cortical representations for adjacent fingertips in S1 of
822 individual subjects: Finger Representation Overlap in S1 at 7T. *Human Brain Mapping*, 35(5),
823 2027–2043.
- 824 Biermann, K., Schmitz, F., Witte, O. W., Konczak, J., Freund, H.-J., & Schnitzler, A. (1998). Interaction
825 of finger representation in the human first somatosensory cortex: a neuromagnetic study.
826 *Neuroscience Letters*, Vol. 251, pp. 13–16. doi:10.1016/s0304-3940(98)00480-7
- 827 Brochier, T., Boudreau, M. J., Paré, M., & Smith, A. M. (1999). The effects of muscimol inactivation of
828 small regions of motor and somatosensory cortex on independent finger movements and
829 force control in the precision grip. *Experimental Brain Research. Experimentelle
830 Hirnforschung. Experimentation Cerebrale*, 128(1–2), 31–40.
- 831 Brodmann, K. (1909). *Vergleichende Lokalisationslehre der Grosshirnrinde in ihren Prinzipien
832 dargestellt auf Grund des Zellenbaues*. Barth.
- 833 Brouwer, G. J., Arnedo, V., Offen, S., Heeger, D. J., & Grant, A. C. (2015). Normalization in human
834 somatosensory cortex. *Journal of Neurophysiology*, 114(5), 2588–2599.
- 835 Carandini, M., & Heeger, D. J. (2011). Normalization as a canonical neural computation. *Nature
836 Reviews. Neuroscience*, 13(1), 51–62.
- 837 Carlson, M. (1981). Characteristics of sensory deficits following lesions of Brodmann's areas 1 and 2
838 in the postcentral gyrus of Macaca mulatta. *Brain Research*, 204(2), 424–430.
- 839 Chemnitz, A., Dahlin, L. B., & Carlsson, I. K. (2013). Consequences and adaptation in daily life –
840 patients' experiences three decades after a nerve injury sustained in adolescence. *BMC
841 Musculoskeletal Disorders*, 14(1), 1–9.

- 842 Cole, K. J., & Abbs J. H. (1988). Grip force adjustments evoked by load force perturbations of a
843 grasped object. *Journal of Neurophysiology*, 60(4), 1513-22.
- 844 Crevecoeur, F., Barrea, A., Libouton, X., Thonnard, J.-L., & Lefèvre, P. (2017). Multisensory
845 components of rapid motor responses to fingertip loading. *Journal of Neurophysiology*,
846 118(1), 331–343.
- 847 Darian-Smith, C., & Darian-Smith, I. (1993). Thalamic projections to areas 3a, 3b, and 4 in the
848 sensorimotor cortex of the mature and infant macaque monkey. *The Journal of Comparative
849 Neurology*, 335(2), 173–199.
- 850 Diedrichsen, J., Berlot, E., Mur, M., Schütt, H. H., & Kriegeskorte, N. (2020). Comparing
851 representational geometries using the unbiased distance correlation. Retrieved from
852 <http://arxiv.org/abs/2007.02789>
- 853 Diedrichsen, J., & Kriegeskorte, N. (2017). Representational models: A common framework for
854 understanding encoding, pattern-component, and representational-similarity analysis. *PLoS
855 Computational Biology*, 13(4), e1005508.
- 856 Diedrichsen, J., Provost, S., & Zareamoghaddam, H. (2016). On the distribution of cross-validated
857 Mahalanobis distances. Retrieved from <http://arxiv.org/abs/1607.01371>
- 858 Ejaz, N., Hamada, M., & Diedrichsen, J. (2015). Hand use predicts the structure of representations in
859 sensorimotor cortex. *Nature Neuroscience*, 18(7), 1034–1040.
- 860 Fischl, B., Sereno, M. I., & Dale, A. M. (1999). Cortical surface-based analysis. II: Inflation, flattening,
861 and a surface-based coordinate system. *NeuroImage*, 9(2), 195–207.
- 862 Fischl, B., Rajendran, N., Busa, E., Augustinack, J., Hinds, O., Yeo, B. T. T., ... Zilles, K. (2008). Cortical
863 folding patterns and predicting cytoarchitecture. *Cerebral Cortex*, 18(8), 1973–1980.
- 864 Florence, S. L., Wall, J. T., & Kaas, J. H. (1988). The somatotopic pattern of afferent projections from
865 the digits to the spinal cord and cuneate nucleus in macaque monkeys. *Brain Research*,
866 452(1–2), 388–392.
- 867 Florence, S. L., Wall, J. T., & Kaas, J. H. (1989). Somatotopic organization of inputs from the hand to
868 the spinal gray and cuneate nucleus of monkeys with observations on the cuneate nucleus
869 of humans. *The Journal of Comparative Neurology*, 286(1), 48–70.
- 870 Friedman, R. M., Chen, L. M., & Roe, A. W. (2008). Responses of areas 3b and 1 in anesthetized
871 squirrel monkeys to single- and dual-site stimulation of the digits. *Journal of
872 Neurophysiology*, 100(6), 3185–3196.
- 873 Friston, K. J., Jezzard, P., & Turner, R. (1994). Analysis of functional MRI time-series. *Human Brain
874 Mapping*, Vol. 1, pp. 153–171. doi:10.1002/hbm.460010207

- 875 Gale, D. J., Flanagan, R. J., & Gallivan, J. P. (2021). Human somatosensory cortex is modulated
876 during motor planning. *The Journal of Neuroscience: The Official Journal of the Society for
877 Neuroscience*. doi:10.1523/JNEUROSCI.0342-21.2021
- 878 Gandevia, S. C., Burke, D., & McKeon, B. B. (1983). Convergence in the somatosensory pathway
879 between cutaneous afferents from the index and middle fingers in man. *Experimental Brain
880 Research. Experimentelle Hirnforschung. Experimentation Cerebrale*, 50(2–3), 415–425.
- 881 Geyer, S., Ledberg, A., Schleicher, A., Kinomura, S., Schormann, T., Bürgel, U., ... Roland, P. E. (1996).
882 Two different areas within the primary motor cortex of man. *Nature*, 382(6594), 805–807.
- 883 Ghosh, S., Brinkman, C., & Porter, R. (1987). A quantitative study of the distribution of neurons
884 projecting to the precentral motor cortex in the monkey (M. fascicularis). *The Journal of
885 Comparative Neurology*, 259(3), 424–444.
- 886 Goldring, A. B., Cooke, D. F., Baldwin, M. K. L., Recanzone, G. H., Gordon, A. G., Pan, T., ... Krubitzer,
887 L. (2014). Reversible deactivation of higher-order posterior parietal areas. II. Alterations in
888 response properties of neurons in areas 1 and 2. *Journal of Neurophysiology*, 112(10), 2545–
889 2560.
- 890 Häger-Ross, C., Cole, K. J., & Johansson, R. S. (1996). Grip-force responses to unanticipated object
891 loading: load direction reveals body- and gravity-referenced intrinsic task variables.
892 *Experimental Brain Research. Experimentelle Hirnforschung. Experimentation Cerebrale*,
893 110(1), 142–150.
- 894 Hernandez-Castillo, C. R., Maeda, R. S., Pruszynski, J. A., & Diedrichsen, J. (2020). Sensory
895 information from a slipping object elicits a rapid and automatic shoulder response. *Journal
896 of Neurophysiology*, 123(3), 1103–1112.
- 897 Hikosaka, O., Tanaka, M., Sakamoto, M., & Iwamura, Y. (1985). Deficits in manipulative behaviors
898 induced by local injections of muscimol in the first somatosensory cortex of the conscious
899 monkey. *Brain Research*, 325(1–2), 375–380.
- 900 Hoechstetter, K., Rupp, A., Stančák, A., Meinck, H.-M., Stippich, C., Berg, P., & Scherg, M. (2001).
901 Interaction of Tactile Input in the Human Primary and Secondary Somatosensory Cortex—A
902 Magnetoencephalographic Study. *NeuroImage*, 14(3), 759–767.
- 903 Hsiao, S. S., O'Shaughnessy, D. M., & Johnson, K. O. (1993). Effects of selective attention on spatial
904 form processing in monkey primary and secondary somatosensory cortex. *Journal of
905 Neurophysiology*, 70(1), 444–447.
- 906 Hsieh, C.-L., Shima, F., Tobimatsu, S., Sun, S.-J., & Kato, M. (1995). The interaction of the
907 somatosensory evoked potentials to simultaneous finger stimuli in the human central
908 nervous system. A study using direct recordings. *Electroencephalography and Clinical
909 Neurophysiology*, 96(2), 125–132.

- 909 *Neurophysiology/Evoked Potentials Section*, Vol. 96, pp. 135–142. doi:10.1016/0168-
910 5597(94)00251-9

911 Hutton, C., Bork, A., Josephs, O., Deichmann, R., Ashburner, J., & Turner, R. (2002). Image distortion
912 correction in fMRI: A quantitative evaluation. *NeuroImage*, 16(1), 217–240.

913 Hyvärinen, J., & Poranen, A. (1978a). Movement-sensitive and direction and orientation-selective
914 cutaneous receptive fields in the hand area of the post-central gyrus in monkeys. *The
915 Journal of Physiology*, 283(1), 523–537.

916 Hyvärinen, J., & Poranen, A. (1978b). Receptive field integration and submodality convergence in
917 the hand area of the post-central gyrus of the alert monkey. *The Journal of Physiology*, Vol.
918 283, pp. 539–556. doi:10.1113/jphysiol.1978.sp012518

919 Ishibashi, H., Tobimatsu, S., Shigeto, H., Morioka, T., Yamamoto, T., & Fukui, M. (2000). Differential
920 interaction of somatosensory inputs in the human primary sensory cortex: a
921 magnetoencephalographic study. *Clinical Neurophysiology: Official Journal of the
922 International Federation of Clinical Neurophysiology*, 111(6), 1095–1102.

923 Iwamura, Y. (1998). Hierarchical somatosensory processing. *Current Opinion in Neurobiology*, 8(4),
924 522–528.

925 Iwamura, Y., Tanaka, M., Sakamoto, M., & Hikosaka, O. (1993). Rostrocaudal gradients in the
926 neuronal receptive field complexity in the finger region of the alert monkey's postcentral
927 gyrus. *Experimental Brain Research. Experimentelle Hirnforschung. Experimentation
928 Cerebrale*, 92(3), 360–368.

929 Jones, E. G. (1975). Lamination and differential distribution of thalamic afferents within the sensory-
930 motor cortex of the squirrel monkey. *The Journal of Comparative Neurology*, 160(2), 167–
931 203.

932 Jones, E. G., & Powell, T. P. (1970). Connexions of the somatic sensory cortex of the rhesus monkey.
933 3. Thalamic connexions. *Brain: A Journal of Neurology*, 93(1), 37–56.

934 Krause, T., Kurth, R., Ruben, J., Schwiemann, J., Villringer, K., Deuchert, M., ... Villringer, A. (2001).
935 Representational overlap of adjacent fingers in multiple areas of human primary
936 somatosensory cortex depends on electrical stimulus intensity: an fMRI study. *Brain
937 Research*, 899(1–2), 36–46.

938 Laboy-Juárez, K. J., Langberg, T., Ahn, S., & Feldman, D. E. (2019). Elementary motion sequence
939 detectors in whisker somatosensory cortex. *Nature Neuroscience*, 22(9), 1438–1449.

940 Lipton, M. L., Liszewski, M. C., Noelle O'Connell, M., Mills, A., Smiley, J. F., Branch, C. A., ... Schroeder,
941 C. E. (2010). Interactions within the Hand Representation in Primary Somatosensory Cortex of

- Primates. *The Journal of Neuroscience: The Official Journal of the Society for Neuroscience*, 30(47), 15895–15903.

Lyall, E. H., Mossing, D. P., Pluta, S. R., Chu, Y. W., Dudai, A., & Adesnik, H. (2021). Synthesis of a comprehensive population code for contextual features in the awake sensory cortex. *eLife*, doi:10.7554/eLife.62687

Martuzzi, R., van der Zwaag, W., Farthouat, J., Gruetter, R., & Blanke, O. (2014). Human finger somatotopy in areas 3b, 1, and 2: a 7T fMRI study using a natural stimulus: Human Finger Somatotopy in Areas 3b, 1, and 2. *Human Brain Mapping*, 35(1), 213–226.

Moberg, E. (1958). Objective methods for determining the functional value of sensibility in the hand. *The Journal of Bone and Joint Surgery. British Volume*. doi:10.1302/0301-620X.40B3.454

Monzée, J., Lamarre, Y., & Smith, A. M. (2003). The effects of digital anesthesia on force control using a precision grip. *Journal of Neurophysiology*, 89(2), 672–683.

Naselaris, T., Kay, K. N., Nishimoto, S., & Gallant, J. L. (2011). Encoding and decoding in fMRI. *NeuroImage*, 56(2), 400–410.

Nili, H., Wingfield, C., Walther, A., Su, L., Marslen-Wilson, W., & Kriegeskorte, N. (2014). A toolbox for representational similarity analysis. *PLoS Computational Biology*, 10(4), e1003553.

Ohki, Y., Edin, B. B., & Johansson, R. S. (2002). Predictions specify reactive control of individual digits in manipulation. *The Journal of Neuroscience: The Official Journal of the Society for Neuroscience*, 22(2), 600–610.

Oosterhof, N. N., Wiestler, T., Downing, P. E., & Diedrichsen, J. (2011). A comparison of volume-based and surface-based multi-voxel pattern analysis. *NeuroImage*, 56(2), 593–600.

Phillips, J. R., Johnson, K. O., & Hsiao, S. S. (1988). Spatial pattern representation and transformation in monkey somatosensory cortex. *Proceedings of the National Academy of Sciences of the United States of America*, 85(4), 1317–1321.

Powell, T. P., & Mountcastle, V. B. (1959). The cytoarchitecture of the postcentral gyrus of the monkey Macaca mulatta. *Bulletin of the Johns Hopkins Hospital*, 105, 108–131.

Rathelot, J.-A., & Strick, P. L. (2009). Subdivisions of primary motor cortex based on cortico-motoneuronal cells. *Proceedings of the National Academy of Sciences of the United States of America*, 106(3), 918–923.

Reed, J. L., Pouget, P., Qi, H.-X., Zhou, Z., Bernard, M. R., Burish, M. J., ... Kaas, J. H. (2008). Widespread spatial integration in primary somatosensory cortex. *Proceedings of the National Academy of Sciences of the United States of America*, 105(29), 10233–10237.

- 975 Reed, J. L., Qi, H.-X., Zhou, Z., Bernard, M. R., Burish, M. J., Bonds, A. B., & Kaas, J. H. (2010).
976 Response properties of neurons in primary somatosensory cortex of owl monkeys reflect
977 widespread spatiotemporal integration. *Journal of Neurophysiology*, 103(4), 2139–2157.
- 978 Ruben, J., Krause, T., Taskin, B., Blankenburg, F., Moosmann, M., & Villringer, A. (2006). Sub-area-
979 specific Suppressive Interaction in the BOLD responses to simultaneous finger stimulation in
980 human primary somatosensory cortex: evidence for increasing rostral-to-caudal convergence.
981 *Cerebral Cortex*, 16(6), 819–826.
- 982 Shanks, M. F., & Powell, T. P. (1981). An electron microscopic study of the termination of
983 thalamocortical fibres in areas 3b, 1 and 2 of the somatic sensory cortex in the monkey.
984 *Brain Research*, 218(1–2), 35–47.
- 985 Sur, M. (1980). Receptive fields of neurons in areas 3b and 1 of somatosensory cortex in monkeys.
986 *Brain Research*, 198(2), 465–471.
- 987 Thakur, P. H., Fitzgerald, P. J., & Hsiao, S. S. (2012). Second-order receptive fields reveal multidigit
988 interactions in area 3b of the macaque monkey. *Journal of Neurophysiology*, 108(1), 243–
989 262.
- 990 Walther, A., Nili, H., Ejaz, N., Alink, A., Kriegeskorte, N., & Diedrichsen, J. (2016). Reliability of
991 dissimilarity measures for multi-voxel pattern analysis. *NeuroImage*, 137, 188–200.
- 992 Yau, J. M., Connor, C. E., & Hsiao, S. S. (2013). Representation of tactile curvature in macaque
993 somatosensory area 2. *Journal of Neurophysiology*, 109(12), 2999–3012.
- 994 Yau, J. M., Kim, S. S., Thakur, P. H., & Bensmaia, S. J. (2016). Feeling form: the neural basis of haptic
995 shape perception. *Journal of Neurophysiology*, 115(2), 631–642.
- 996 Yousry, T. A., Schmid, U. D., Alkadhi, H., Schmidt, D., Peraud, A., Buettner, A., & Winkler, P. (1997).
997 Localization of the motor hand area to a knob on the precentral gyrus. A new landmark.
998 *Brain: A Journal of Neurology*, 120 (Pt 1), 141–157.
- 999

1000 Figure legends

1001 **Figure 1. Experiment design.** (a) Participants experienced tactile stimulation using a custom-built finger
1002 stimulation box. Each finger was independently restrained, and pneumatic pistons were used to deliver
1003 stimulation to each fingertip. (b) Schematic illustration of a single trial (ITI: inter-trial-interval). The blue trace
1004 shows the mean finger stimulation force (\pm SEM across participants), time aligned to the start of the
1005 stimulation phase. (c) Participants experienced stimulation of all 31 possible single- and multi-finger
1006 combinations.

1007

1008 **Figure 2. Activation and representation of fingers in sensorimotor cortex.** (a) Group-average percent signal
1009 change (relative to resting baseline) across all 31 possible finger combinations, projected to a flattened view
1010 of the left cortical sensorimotor areas around the central sulcus. Approximate boundaries of
1011 cytoarchitectonic areas (Fischl et al., 2008) are indicated by white dotted lines. The gray background
1012 indicates the average sulcal depth, with gyri in light, and sulci in dark colors. The rectangle indicates the area
1013 of averaging in the cross-sections in B and D. The scale bar approximates 1cm on the flattened surface. (b)
1014 Cross-sectional profiles of the average percent signal change (\pm SEM across participants) within the dashed
1015 rectangle in A, grouped by the number of fingers in each combination. The x-axis corresponds to the
1016 approximate spatial location along the rostral-caudal axis spanned by the rectangular box on the cortical
1017 surface. Vertical dashed lines mark the approximate boundaries between Brodmann areas. (c) Cortical surface
1018 map of the average crossnibus dissimilarity between activity patterns evoked by single-finger stimulation. (d)
1019 Cross-sectional profiles of the average crossnibus dissimilarity (\pm SEM across participants) between pairs of
1020 single-finger, 2-finger, 3-finger, or 4-finger combinations.

1021

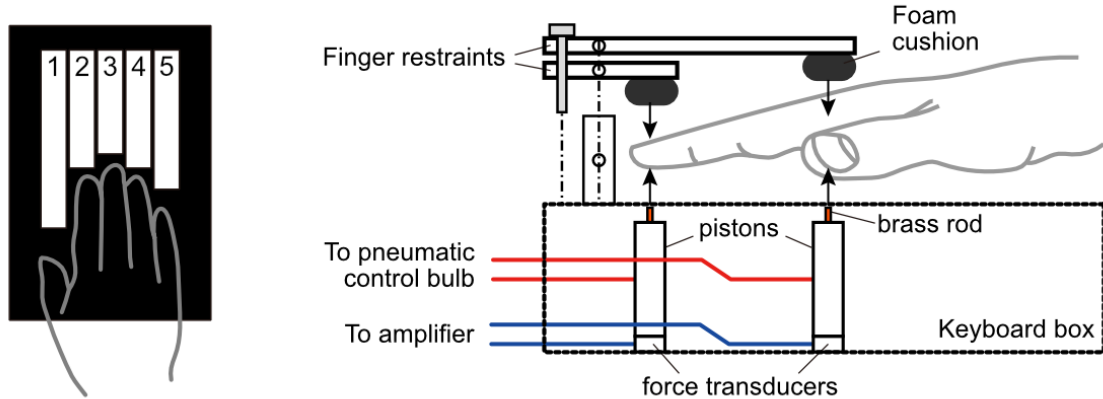
1022 **Figure 3. Finger tuning in sensorimotor cortex.** (a) Activity patterns for each of the five fingers from one
1023 participant, projected onto a flattened cortical surface and cut to include BA 3a to BA 2 in each panel. (b)
1024 Average scaled voxel tuning curves arranged by most preferred finger (denoted by the gray box). Each colour
1025 corresponds to different regions. (c) Finger selectivity coefficients per region. Light gray lines reflect selectivity
1026 coefficients per participant, and solid black line reflects the average across participants. The lower dashed line
1027 reflects the average expected selectivity if voxels were randomly tuned to fingers, while the upper dashed line
1028 reflects the average expected selectivity if voxels only responded to a single finger. Expected values take into
1029 account the empirical noise variance in each region and participant. A-priori paired t-tests were conducted

1030 between normalized selectivity coefficients (see Methods) from different regions, and lines above the plot
1031 denote significant differences. Error bars in B and C reflect SEM across participants in each region.

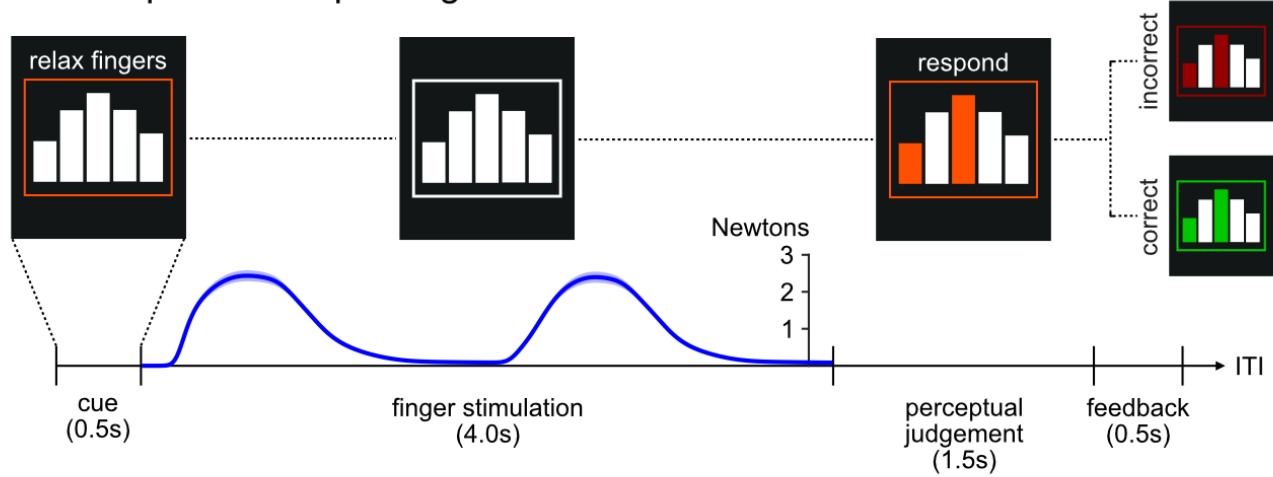
1032

1033 **Figure 4. Multi-finger activity patterns in sensorimotor cortex.** (a) Exemplar activity patterns from the
1034 participants displayed in Figure 3A. (b) Representational model fits were normalized to the null model (0) and
1035 the noise-ceiling (1) in each region in each participant. Dots reflect the mean and error bars reflect SEM
1036 across participants per region. (c) Surface map of the linear model fit (median across participants) in tessels
1037 where there were significant differences between all finger combination patterns (average paired
1038 dissimilarities between finger combination patterns ≥ 0.005). (d) Difference between the fits of the 2-finger
1039 interaction model and the linear model in each tessell (median across participants). (e) Difference between the
1040 noise-ceiling and the fit of the 2-finger interaction model in each tessell. Note that the colour scale for C is
1041 different than that for D and E. (f) The full 2-finger interaction model (red line) was compared to a model
1042 that only contained the adjacent (black markers) or the non-adjacent (white markers) finger-pairs. Asterisks
1043 denote significantly lower model fits compared to using all two-finger interactions (two-sided paired t-test,
1044 $p < 0.05$).

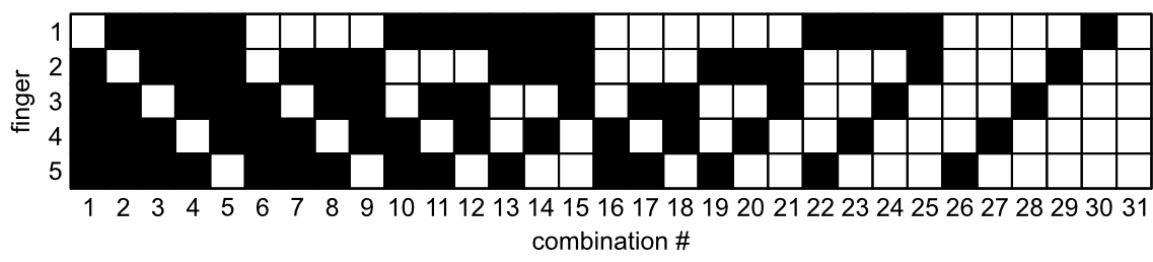
A Finger stimulation device

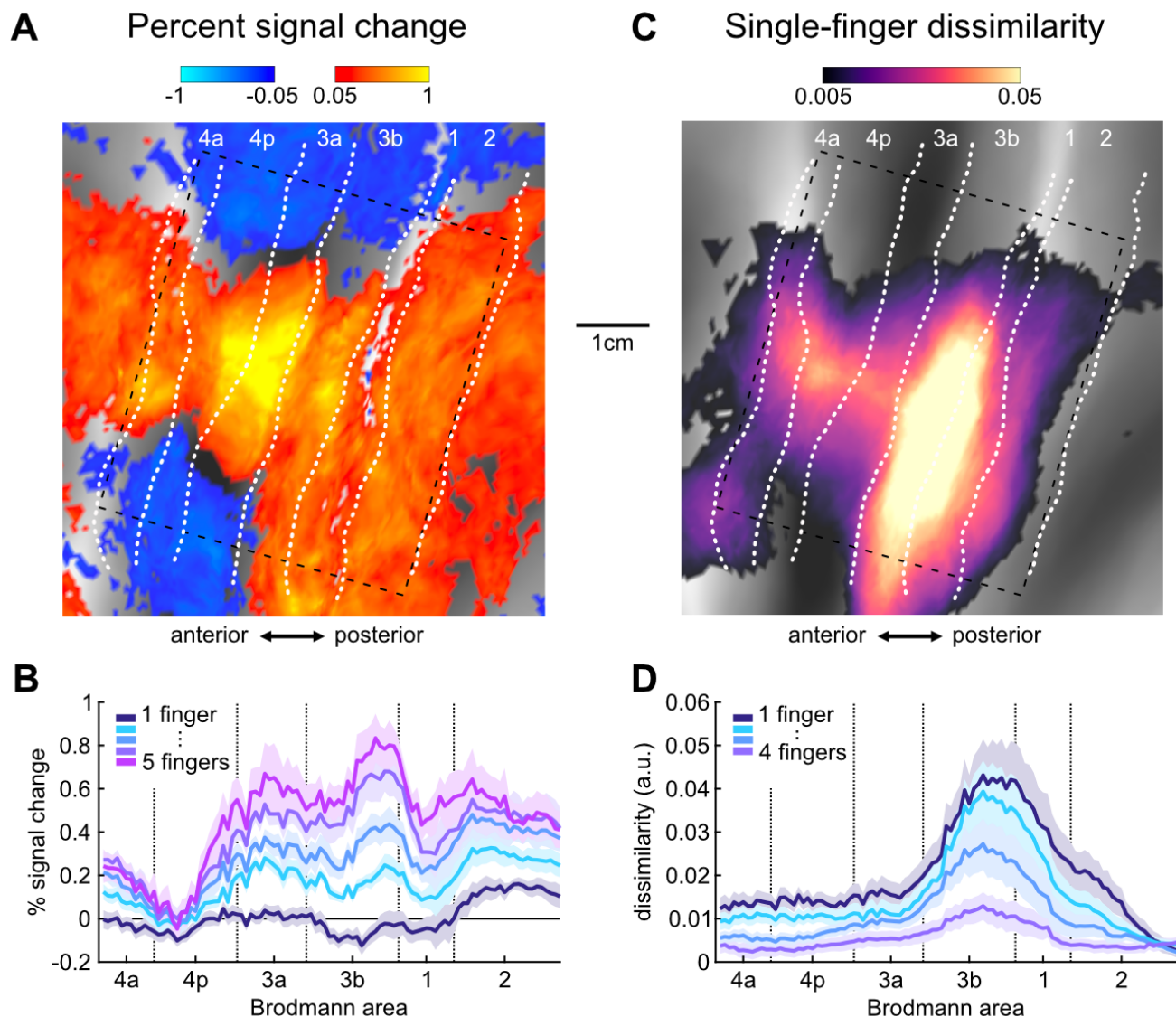


B Experimental paradigm

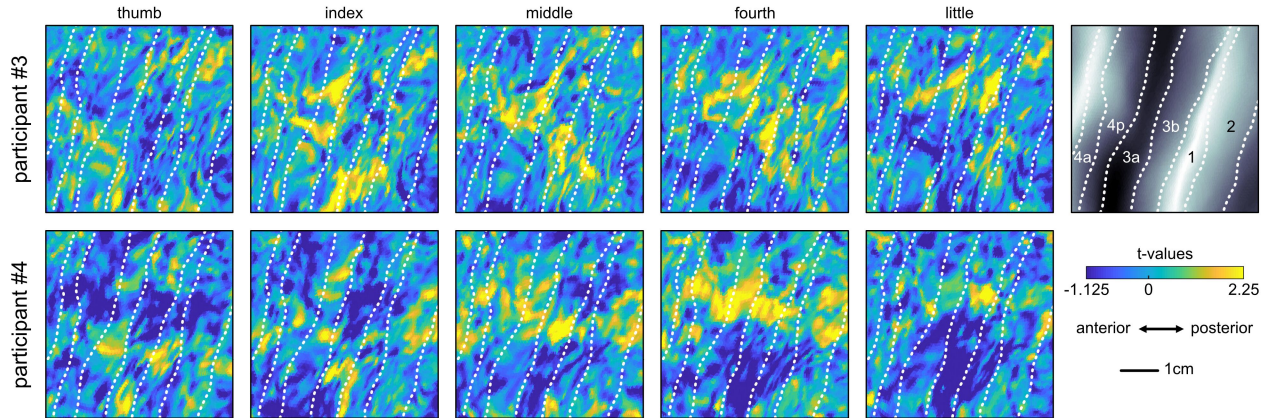


C Finger combinations

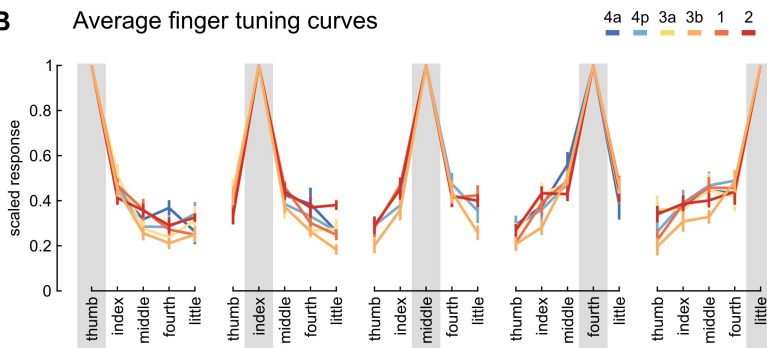




A Single-finger activity patterns



B Average finger tuning curves



C Average finger selectivity

